ACS NANO

www.acsnano.org

ARTICLE

Antioxidative Hyaluronic Acid–Bilirubin Nanomedicine Targeting Activated Hepatic Stellate Cells for Anti-Hepatic-Fibrosis Therapy

Jongyoon Shinn,[▽] Seojeong Park,[▽] Seonju Lee, Nayoon Park, Seojeong Kim, Seohui Hwang, James J. Moon, Youngjoo Kwon,* and Yonghyun Lee*

Cite This: *ACS Nano* 2024, 18, 4704–4716

Read Online

ACCESS | Metrics & More | Article Recommendations | Supporting Information

ABSTRACT: **Liver fibrosis is a life-threatening and irreversible disease. The fibrosis process is largely driven by hepatic stellate cells (HSCs), which undergo transdifferentiation from an inactivated state to an activated one during persistent liver damage. This activated state is responsible for collagen deposition in liver tissue and is accompanied by increased CD44 expression on the surfaces of HSCs and amplified intracellular oxidative stress, which contributes to the fibrosis process. To address this problem, we have developed a strategy that combines CD44-targeting of activated HSCs with an antioxidative approach. We developed hyaluronic acid–bilirubin nanoparticles (HABNs), composed of endogenous bilirubin, an antioxidant and anti-inflammatory bile acid, and hyaluronic acid, an endogenous CD44-targeting glycosaminoglycan biopolymer. Our findings demonstrate that intravenously administered HABNs effectively targeted the liver, particularly activated HSCs, in fibrotic mice with choline-deficient L-amino acid-defined high-fat diet (CD-HFD)-induced nonalcoholic steatohepatitis (NASH). HABNs were able to inhibit HSC activation and proliferation and collagen production. Furthermore, in a murine CD-HFD-induced NASH fibrosis model, intravenously administered HABNs showed potent fibrotic modulation activity. Our study suggests that HABNs have the potential to serve as a targeted anti-hepatic-fibrosis therapy by modulating activated HSCs via CD44-targeting and antioxidant strategies. This strategy could also be applied to various ROS-related diseases in which CD44-overexpressing cells play a pivotal role.**

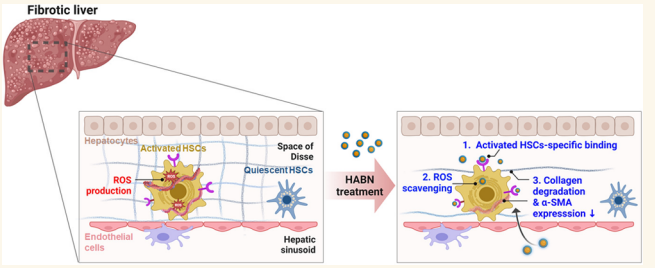

KEYWORDS: *Anti-liver-fibrosis therapy, Antioxidative therapy, Activated hepatic stellate cells, Bilirubin, Hyaluronic acid, Nanomedicine, Nonalcoholic steatohepatitis, NASH*

INTRODUCTION

Liver fibrosis is a severe and life-threatening disease.[1] In response to liver damage, hepatic stellate cells (HSCs) are activated at the injury site, initiating a wound-healing process by generating extracellular matrix (ECM) proteins such as collagen and fibronectin[1,2] However, persistent damage leads to an excessive accumulation of ECM proteins, resulting in liver fibrosis, which is characterized by disrupted liver architecture and impaired functioning.[3,4] The excessive deposition of ECM proteins can lead to the development of irreversible cirrhosis. Cirrhosis patients typically experience severe complications including portal hypertension and liver failure with a high likelihood of developing hepatocellular carcinoma in the end stage.[5−7] Unfortunately, liver transplantation is the only way to treat end-stage hepatic fibrosis.[8]

Activated HSCs play a critical role in liver fibrosis by depositing ECM, making them a promising target for antifibrotic therapy.[2] Various strategies have been developed to modulate HSCs, including targeting specific molecules overexpressed on their surfaces such as the type VI collagen receptor[9,10] and CD44.[11−16] Reactive oxygen species (ROS) also have an important role in the liver fibrosis[17−22] because ROS are critical in promoting HSC activation,[23,24] prolifer-

Received: July 5, 2023
Revised: January 18, 2024
Accepted: January 22, 2024
Published: January 30, 2024

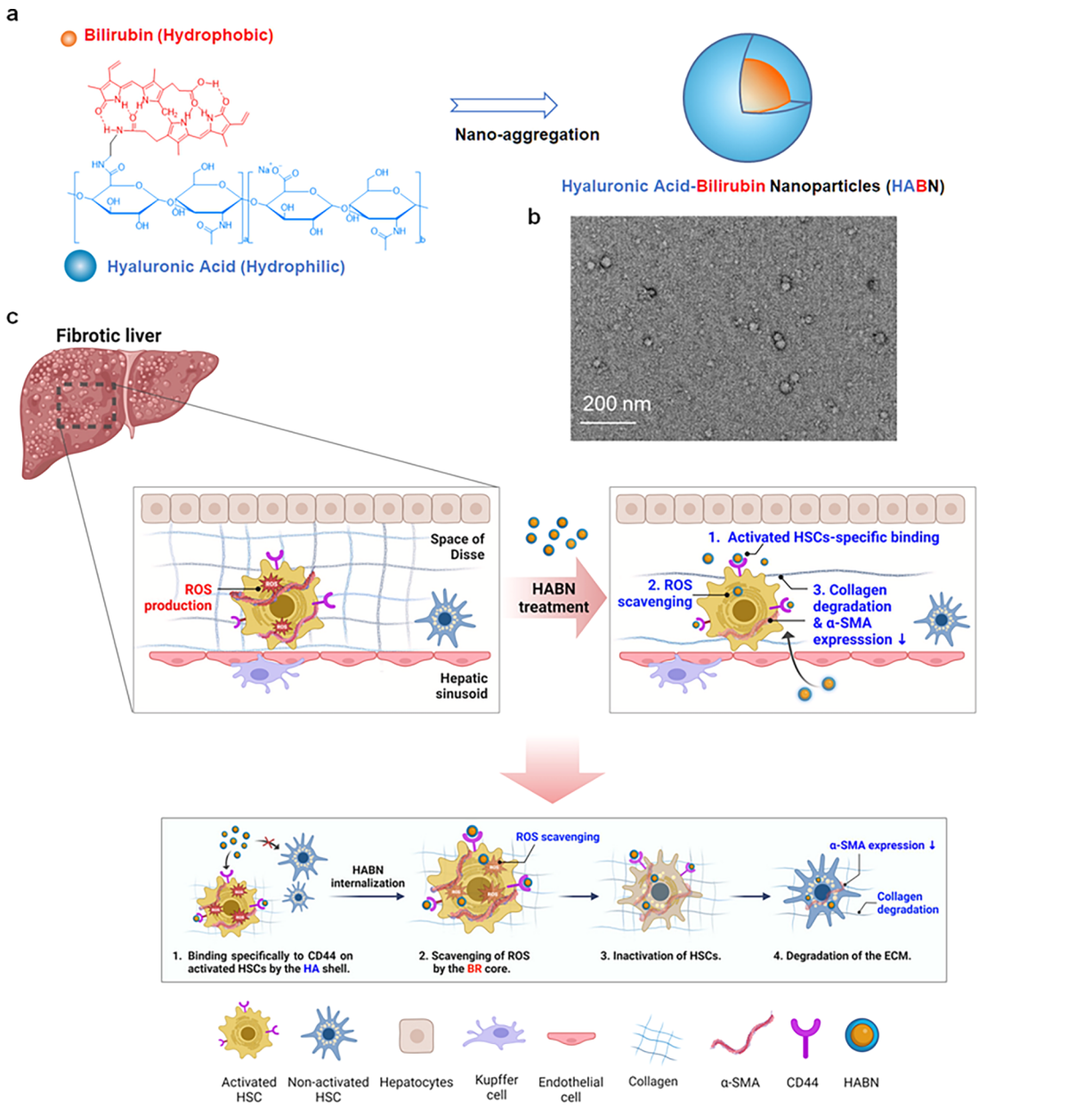

Figure 1. CD44-targeting, antioxidative hyaluronic acid−bilirubin nanoparticles (HABNs) for treating liver fibrosis. (a) Schematic of the self-assembly of HABNs from the hyaluronic acid−bilirubin conjugate. (b) TEM image of HABNs. Scale bar: 200 nm. (c) Schematic of HABN therapy for liver fibrosis. Antioxidant, CD44-targeting HABNs specifically inhibit the oxidative stress of activated HSCs, resulting in the suppression of HSC activity and collagen generation, thereby preventing the progression of liver fibrosis.

ation,[25] and migration[9,21] and collagen synthesis.[21,25] Therefore, modulating activated HSCs by addressing oxidative stress is a potentially valuable therapeutic target.[26,27] However, the paradoxical roles of ROS in liver fibrosis require specific modulation of activated HSCs.[28,29] While previous studies have sought to address this challenge by developing nanomedicines with HSC- or ROS-modulating activities,[12,14−16,30−32] they require the use of various experimental drugs as well as complex nanoparticle carriers, thus significantly limiting their successful clinical translation.

To overcome those limitations, we developed hyaluronic acid−bilirubin nanoparticles (HABNs) as a promising antifibrotic nanomedicine that achieves CD44-targeting and antioxidant modulation. HABNs are composed entirely of naturally occurring, biocompatible, and biodegradable materials: bilirubin (BR), an endogenous antioxidant and anti-inflammatory bile acid,[33−37,12,37] and hyaluronic acid (HA), an endogenous glycosaminoglycan biopolymer that targets the CD44 overexpressed on activated HSCs.[12,37−39] When they were administered to mice intravenously, the HA shell of the HABNs interacted specifically with CD44, enabling them to target activated HSCs in fibrotic livers but not naive HSCs in healthy livers. Moreover, the BR core conferred potent antioxidant activity, contributing to the beneficial modulation of HSCs. Our results demonstrate that HABNs specifically inhibit the oxidative stress in activated HSCs, leading to the suppression of HSC activity and collagen deposition, and consequently effectively prevent the progression of liver fibrosis (Figure 1). Overall, our work demonstrates a biocompatible nanomedicine that can simultaneously target

https://doi.org/10.1021/acsnano.3c06107
ACS Nano 2024, 18, 4704−4716

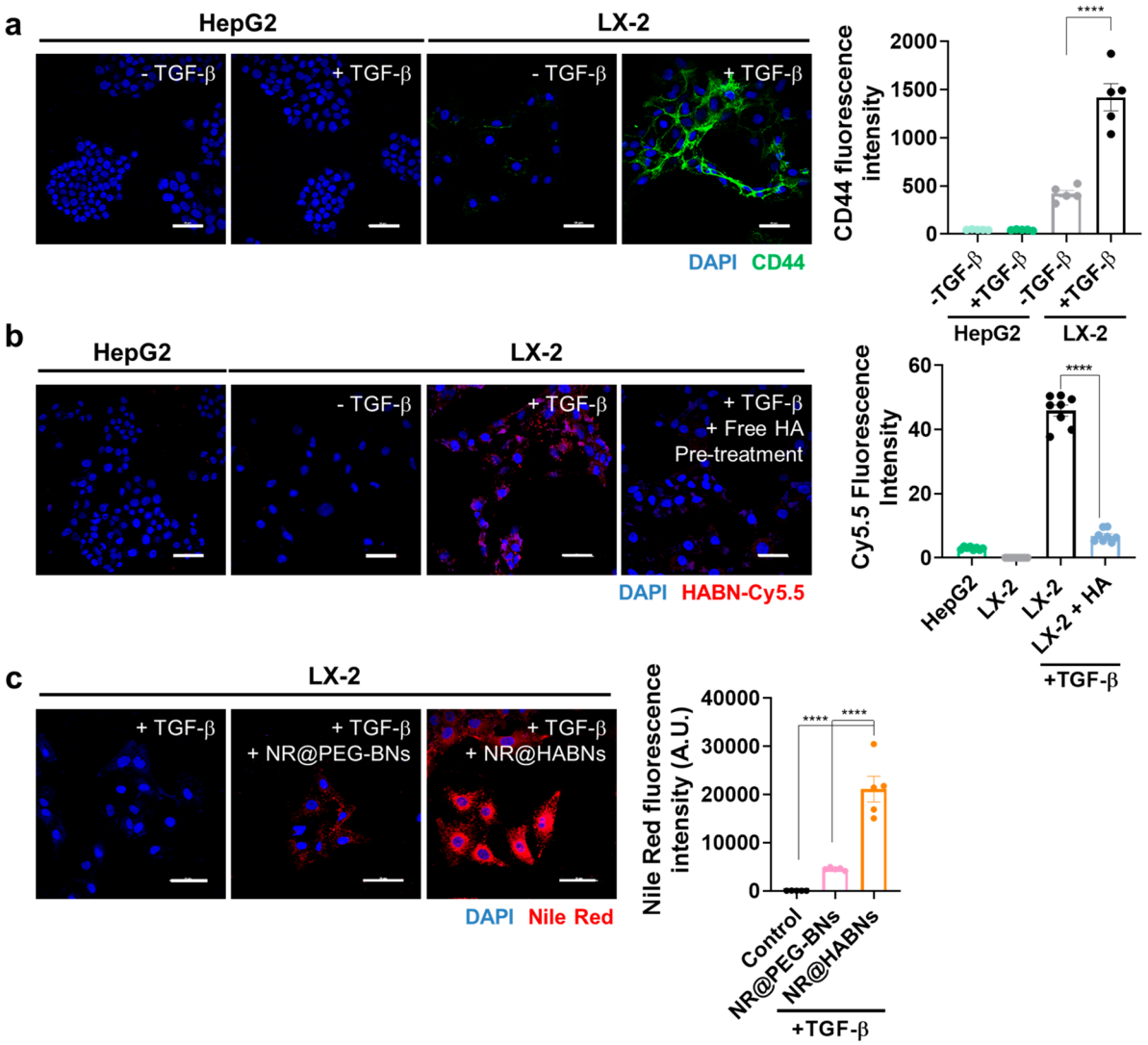

Figure 2. HABNs target activated HSCs. (a) Confocal microscopy images of HepG2 and LX-2 cells preincubated with TGF-β (2 ng/mL) or PBS for 24 h and then stained with anti-CD44−FITC antibody (1/100) for 1 h. (b) Confocal microscopy images and Cy5.5 fluorescence intensities of HepG2 cells and LX-2 cells pretreated with TGF-β (2 ng/mL), TGF-β (2 ng/mL), and free HA (2 mg/mL), or control medium for 24 h, followed by 1 h treatment with HABN−Cy5.5 (30 μg/mL). (c) Confocal microscopy images of LX-2 cells pretreated with TGF-β (2 ng/mL) or control medium for 24 h, followed by 1 h treatment with NR@PEG-BNs (Nile red, 1 μg/mL; PEG-BNs, 62.5 μg/mL) or NR@HABNs (Nile red, 1 μg/mL; HABNs, 62.5 μg/mL). Scale bars: 50 μm. DAPI was used for nucleus counterstaining. Data are presented as mean ± SEM from one representative of three independent experiments with $n = 5$. *$p < 0.05$, **$p < 0.01$, ***$p < 0.001$, ****$p < 0.0001$, analyzed by one-way ANOVA with Tukey's HSD multiple comparison post hoc test.

activated HSCs and control oxidative stress for the treatment of liver fibrosis.

RESULTS

Preparation of Hyaluronic Acid−Bilirubin Nanoparticles from a Hyaluronic Acid−Bilirubin Conjugate. To prepare hyaluronic acid−bilirubin nanoparticles (HABNs), we first synthesized a HA-BR conjugate (Supplementary Figure 1). Even though free BR is a potent antioxidant and cytoprotectant that is quite effective against various systemic diseases, its low solubility has hampered the successful clinical translation and use as a therapeutic.[36,38,40] We hypothesized that conjugating BR with very water-soluble HA would dramatically improve its solubility. As expected, although BR was insoluble in water, the HA-BR conjugates were readily dispersed in an aqueous solution (Supplementary Figure 2a). We also checked how many BR molecules were conjugated with each HA molecule. Our UV/vis analysis revealed an average conjugation density of approximately 4 BR molecules per HA molecule (almost 25 μg/mL of BR in 1 mg/mL of HABNs, Supplementary Figure 2b). HABNs were prepared from the acquired HA-BR conjugate using the film layer method (Supplementary Figure 3a). To investigate whether the HA-BR could self-assemble into a nanostructure, dynamic light scattering (DLS) and transmission electron microscopy (TEM) were used. The DLS analysis showed that the HABNs were 155 ± 83.41 nm (Supplementary Figure 3b), and the TEM results (Figure 1b) showed that the HABNs had a spherical morphology and a size of 84 ± 27.9 nm. The HABNs had a negative zeta-potential (−46.2 ± 4 mV) (Supplementary Figure 3b).

HABNs Target Activated HSCs. HSCs, which have important roles in the fibrosis process, express high levels of CD44 on their surfaces when they are activated.[11] To confirm

https://doi.org/10.1021/acsnano.3c06107
ACS Nano 2024, 18, 4704−4716

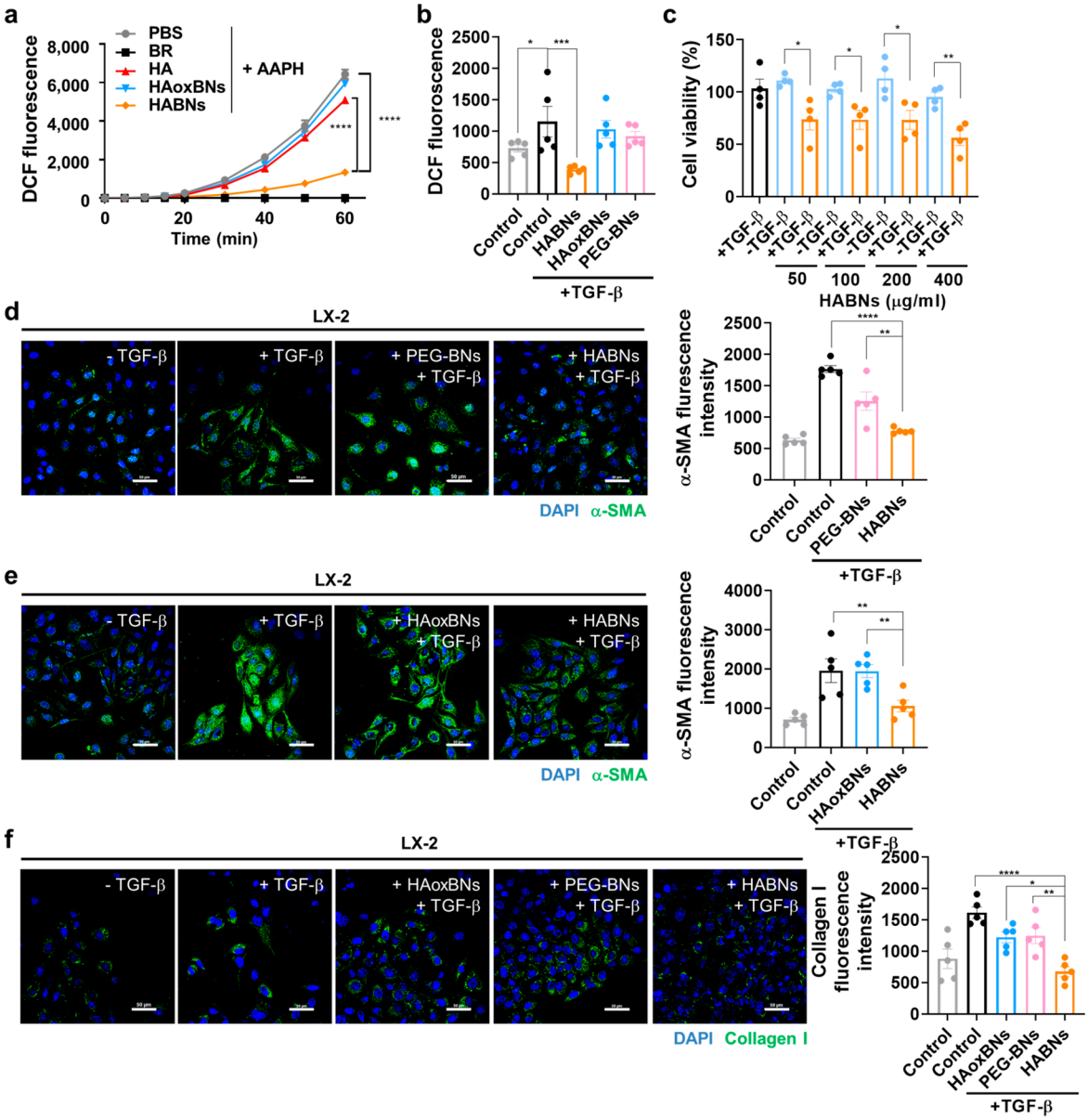

Figure 3. HABNs show antifibrotic activity against activated HSCs *in vitro*. (a) Fluorescence signals of DCF oxidized from DCFDA (50 μM) by peroxyl radicals generated from 1 mM AAPH at 37 °C in the presence of BR (50 μM), HA (1 mg/mL), HAoxBNs (1 mg/mL), HABNs (1 mg/mL), or PBS. (b) Fluorescence signals of intracellular DCF oxidized from DCFDA (30 μM) in LX-2 cells treated with HABNs (0.5 mg/mL), HAoxBNs (0.5 mg/mL), or PEG-BNs (0.5 mg/mL) for 24 h in the absence or presence of TGF-β (2 ng/mL). (c) Viability of LX-2 cells determined with a CCK-8 assay after 24 h of treatment with HABNs (50, 100, 200, or 400 μg/mL) in the absence or presence of TGF-β (2 ng/mL). (d,e) Confocal microscopy images of LX-2 cells treated with (d) PEG-BNs (0.2 mg/mL) or (e) HAoxBNs (0.2 mg/mL) or HABNs (0.2 mg/mL) for 24 h in the absence or presence of TGF-β (2 ng/mL) and then stained with anti-α-SMA antibody (1/100) for 1 h. (f) Confocal microscopy images of LX-2 cells treated with HAoxBNs (0.2 mg/mL), PEG-BNs (0.2 mg/mL), or HABNs (0.2 mg/mL) for 24 h in the absence or presence of TGF-β (2 ng/mL) and then stained with anti-collagen I antibody (1/1000) for 1 h. Scale bars = 50 μm. DAPI was used for nucleus counterstaining. Data are presented as mean ± SEM from one representative of three independent experiments with n = 5. *p < 0.05, **p < 0.01, ***p < 0.001, and ****p < 0.0001, analyzed by two-way ANOVA (a) or one-way ANOVA (b–e) with Tukey's HSD multiple comparison post hoc test (a, c–f) or Fisher's LSD multiple comparison post hoc test (b).

that, we first compared CD44 levels among LX-2 cells (human HSCs), HepG2 cells (normal human hepatocytes), and AML12 cells (normal mouse hepatocytes). CD44 levels on LX-2 cells activated by TGF-β treatment were much higher than those in quiescent LX-2 cells (Figure 2a), which expressed minimal CD44 on their surfaces (Figure 2a). Notably, HepG2 cells did not express any detectable level of CD44, and AML12 cells expressed minimal CD44 on their surfaces (Figure 2a and Supplementary Figure 4a).

Next, we examined whether the CD44-targeting HABNs could specifically bind to CD44 overexpressed on activated LX-2 cells. To do that, we treated HepG2 cells, AML12 cells, quiescent LX-2 cells, and TGF-β-activated LX-2 cells with HABN–Cy5.5. Higher fluorescence signals from HABN–Cy5.5 were observed in TGF-β-activated LX-2 cells than in HepG2 cells, AML12 cells, and quiescent LX-2 cells (Figure 2b and Supplementary Figure 4). Furthermore, free HA pretreatment dramatically decreased the intracellular uptake of HABNs

https://doi.org/10.1021/acsnano.3c06107
ACS Nano 2024, 18, 4704–4716

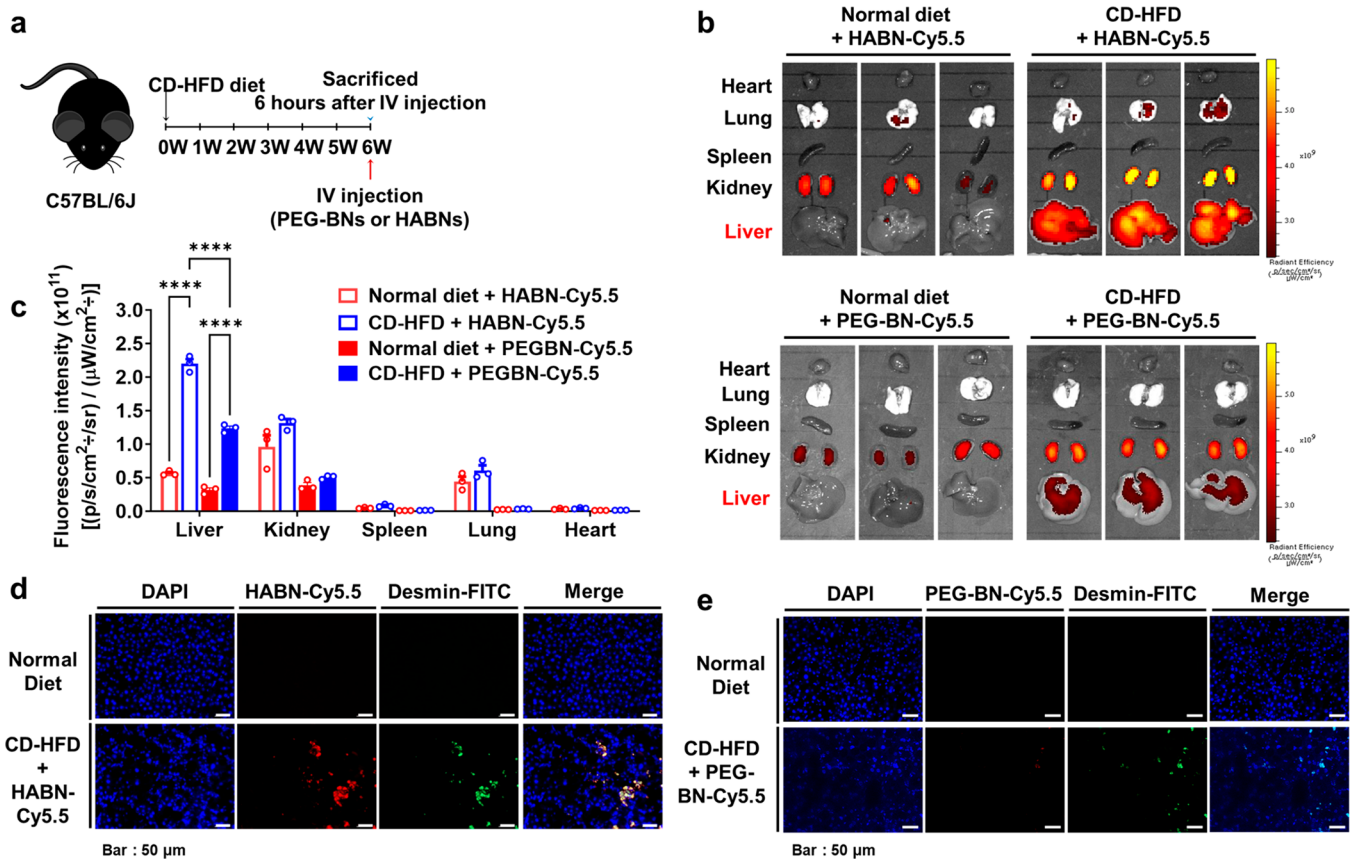

Figure 4. HABNs target activated HSCs in fibrotic livers. (a−c) Six-week-old male C57BL/6 mice fed either a normal diet or a CD-HFD received intravenous (iv) treatment with HABN−Cy5.5 (3.5 mg/kg) or PEG-BN−Cy5.5 (3 mg/kg, equivalent mass of Cy5.5). After 6 h, their organs were imaged by IVIS (b), and the Cy5.5 fluorescence signal was quantified (c). (d,e) Six-week-old male C57BL/6 mice fed a normal diet or a CD-HFD were iv-treated with (d) HABN−Cy5.5 (3.5 mg/kg) or (e) PEG-BN−Cy5.5 (3 mg/kg, equivalent mass of Cy 5.5), and after 6 h, their liver tissues were excised, stained with anti-desmin antibody, and visualized by confocal microscopy. DAPI was applied for nucleus counterstaining. Scale bar: 50 μm. Data are presented as mean ± SEM from a representative of two independent experiments with $n = 3$. ***$p < 0.001$, analyzed by two-way ANOVA with Tukey's HSD multiple comparison post hoc test.

(Figure 2b and Supplementary Figure 4). Indeed, compared with Nile red (NR)-loaded HABNs (NR@HABNs), which were readily internalized into TGF-β-activated LX-2 cells, NR-loaded 20K-PEGylated bilirubin nanoparticles (PEG-BNs) showed a much lower degree of internalization (Figure 2c). These results indicate that the HA shell of the HABNs interacted with CD44 overexpressed on activated HSCs, thus allowing the HABNs to target activated HSCs *in vitro*.

HABNs Show Antifibrotic Activity against Activated HSCs *In Vitro*. Oxidative stress plays an important role in liver fibrogenesis. ROS production is a crucial feature of HSC activation, and ROS can activate HSCs to produce ECM proteins such as collagen.[23−25] Interestingly, HABNs exhibited a more robust ROS-scavenging activity compared with both HA and HAoxBNs, the oxidized form of HABNs (Figure 3a). The primary driver of excessive ECM accumulation in patients with liver fibrosis is HSC activation, and one of the key factors responsible for activating HSCs is TGF-β.[2] TGF-β-activated LX-2 cells are a widely used *in vitro* model for analyzing liver fibrosis.[41−43] We assessed the intracellular ROS production in TGF-β-activated LX-2 cells and the antioxidant activity of HABNs against intracellular ROS. We found that the intracellular 2′,7′-dichlorofluorescein fluorescence in TGF-β-activated LX-2 cells was much stronger than the fluorescence signal in quiescent LX-2 cells, indicating that LX-2 cells activated by TGF-β produced more intracellular ROS than quiescent LX-2 cells (Figure 3b). Intracellular ROS levels in a 3D liver fibrosis spheroid model (HSC spheroids) prepared from AML12 cells and LX-2 cells (24:1) were also increased after TGF-β treatment (Supplementary Figure 5a,b). Moreover, we demonstrated that the antioxidant CD44-targeting HABNs significantly reduced ROS production in activated LX-2 cells overexpressing CD44. On the other hand, the CD44-targeting HAoxBNs and antioxidative PEG-BNs (nontargeted BR nanoparticles) had minimal effects on the intracellular ROS levels in activated LX-2 cells (Figure 3b). HABNs also significantly decreased ROS levels in the TGF-β-activated HSC spheroids, and the HAoxBNs and PEG-BNs did not reduce ROS production (Supplementary Figure 5a,b). These results suggest that intracellular uptake mediated by the HA shell and the subsequent antioxidant activity mediated by the BR core are both crucial to the intracellular ROS-scavenging activity of HABNs in activated HSCs.

Because the oxidative stress caused by activated HSCs is highly associated with the enhanced proliferation of HSCs, the viability of LX-2 cells treated with HABNs was evaluated. No significant toxicity was observed in quiescent LX-2 cells treated with HABN at drug concentrations up to 400 μg/mL (Supplementary Figure 6). Notably, however, activated LX-2 cells treated with HABNs exhibited lower viability than that of

https://doi.org/10.1021/acsnano.3c06107
ACS Nano 2024, 18, 4704−4716

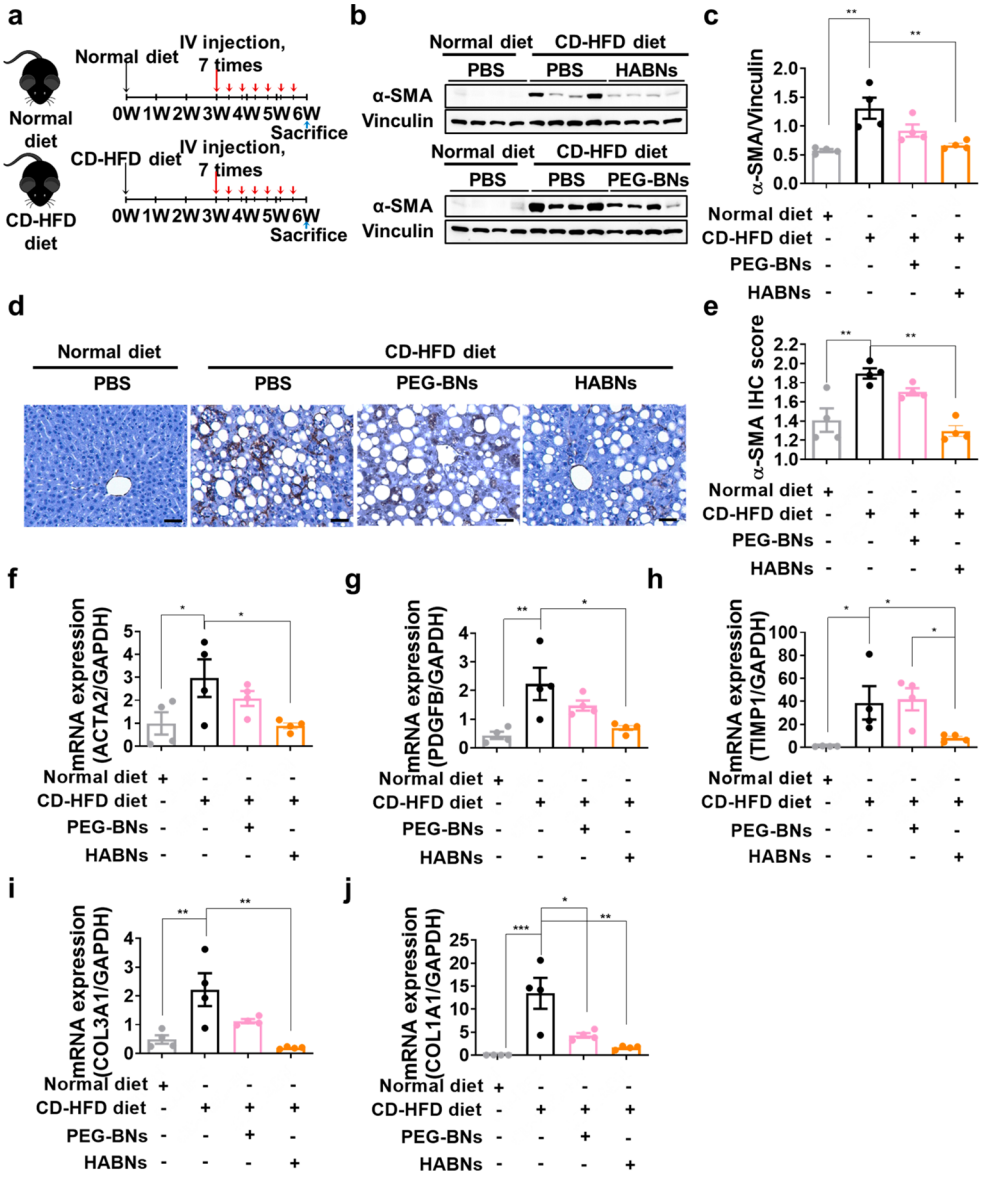

Figure 5. HABNs inhibit the activation of hepatic stellate cells in fibrotic livers *in vivo*. (a–h) Six-week-old male C57BL/6 mice fed a normal diet or a CD-HFD were iv-treated with PBS, PEG-BNs (12 mg/kg), or HABNs (12 mg/kg) every 3 days for a total of 7 times beginning on day 21. On day 42, the animals were euthanized for subsequent analyses. (b,c) α-SMA protein levels extracted from the livers were (b) visualized by Western blotting and (c) quantified using a densitometer. The relative protein expression levels of α-SMA were normalized to vinculin. (d) Liver sections were stained with α-SMA (brown) and hematoxylin (blue) and (e) α-SMA IHC scores were measured. (f–j) mRNA expression levels of fibrogenic genes (*ACTA2*, f; *PDGFB*, g; *TIMP1*, h; *COL3A1*, i; *TIMP1*, j) in the livers were quantified by qRT-PCR. Relative mRNA expression levels were normalized to *GAPDH*. Scale bar: 100 μm. Data are presented as mean ± SEM from a representative of two independent experiments with $n = 4$. $^{*}p < 0.05$, $^{**}p < 0.01$, and $^{***}p < 0.001$, analyzed by one-way ANOVA with Tukey's HSD multiple comparison post hoc test (c, e, g, i, j) or Fisher's LSD multiple comparison post hoc test (f, h).

quiescent LX-2 cells (Figure 3c). These results indicate that HABNs can inhibit proliferation of activated LX-2 cells without exhibiting toxicity against quiescent LX-2 cells.

The expression of α-SMA in HSCs is highly associated with transdifferentiation to a more activated state, making it a marker of HSC activation.[44] An *in vitro* confocal analysis revealed that upon activation by TGF-β, both LX-2 cells and HSC spheroids increased their expression of α-SMA (Figure 3d,e and Supplementary Figure 5c). Notably, HABN treatment significantly reduced the expression of α-SMA in activated HSCs, whereas HAoxBNs and PEG-BNs had minimal effects on α-SMA levels in activated HSCs (Figure 3d,e and Supplementary Figure 5c). These results, together with the antioxidant results, suggest that HABN-mediated reduction in oxidative stress is associated with the inhibition of HSC activation.

Collagens I and III are predominantly deposited among various ECM components in fibrotic livers, and TGF-β-activated HSCs play a pivotal role in the generation of collagens I and III.[45] Excessive accumulation of ECM components such as collagen plays a pivotal role in impairing normal liver architecture and functioning and causing liver fibrosis.[14] Because increased collagen expression is also highly associated with enhanced oxidative stress,[25] we investigated the collagen expression levels in both LX-2 cells and HSC spheroids treated with HAoxBNs, PEG-BNs, or HABNs. An

https://doi.org/10.1021/acsnano.3c06107
ACS Nano 2024, 18, 4704–4716

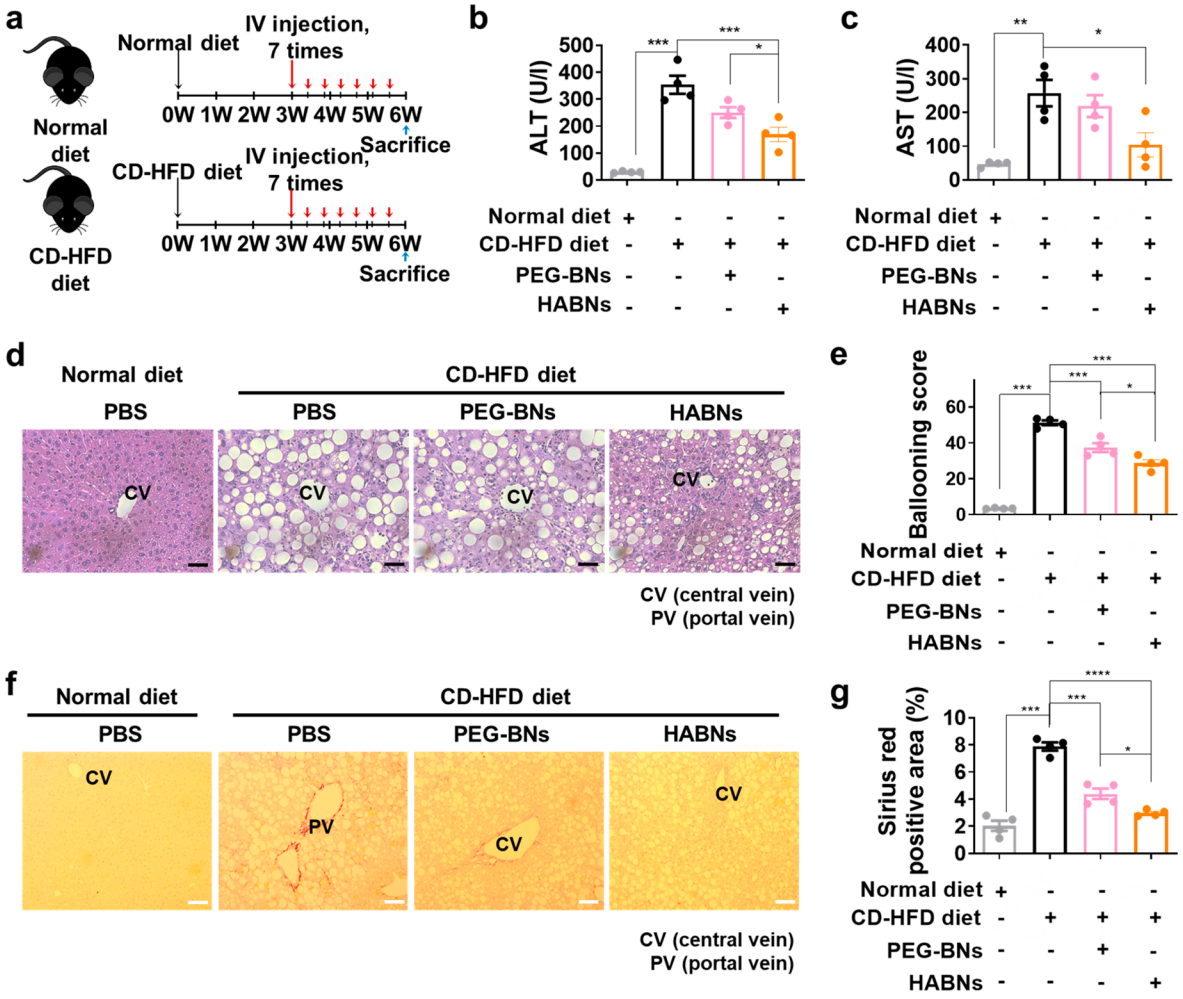

Figure 6. HABNs have potent antifibrotic effects in the CD-HFD-induced NASH fibrosis model. (a−g) Six-week-old C57BL/6J mice fed with a normal diet or a CD-HFD were iv-treated with PBS, PEG-BNs (12 mg/kg), or HABNs (12 mg/kg) every 3 days for a total of 7 times beginning on day 21. (b,c) On day 42, blood was collected from the animals, and liver functional enzyme (ALT, b, and AST, c) levels were measured. (d−g) On day 42, the animals were euthanized. Liver sections were stained with hematoxylin and eosin (d) or Sirius red (f), and ballooning scores (e) and Sirius red-positive areas (g) were measured. CV: central vein. PV: portal vein. Scale bar: 100 μm. Data are presented as mean ± SEM from a representative of two independent experiments with $n = 4$. *$p < 0.05$, **$p < 0.01$, and ***$p < 0.001$, analyzed by one-way ANOVA with Tukey's HSD multiple comparison post hoc test.

in vitro confocal analysis showed that PEG-BNs and HAoxBNs minimally reduced collagen I expression in activated HSCs, probably due to their limited intracellular uptake (caused by the lack of an HA shell) and their very low antioxidant activity (caused by the oxidized BR core), respectively (Figure 3f and Supplementary Figure 5d). Notably, HABNs significantly inhibited the generation of collagen I in activated HSCs, compared with PEG-BNs and HAoxBNs (Figure 3f and Supplementary Figure 5d).

Taken together, our results show that the antioxidant CD44-targeting HABNs can target activated HSCs and reduce their viability and ECM production.

HABNs Accumulate in Activated HSCs in Fibrotic Regions of the Liver *In Vivo*. A murine nonalcoholic steatohepatitis (NASH) model, in which the mice were fed a choline-deficient L-amino acid-defined high-fat diet (CD-HFD), serves as a dietary NASH model with rapidly progressive liver fibrosis. These CD-HFD-fed mice are considered to be a human-relevant NASH-fibrosis model.[41,46] Thus, to determine whether HABNs target fibrotic liver cells, especially activated HSCs, *in vivo*, we intravenously administered PEG-BN−Cy5.5 or HABN−Cy5.5 to mice fed either a CD-HFD or a normal diet (Figure 4a and Supplementary Figure 7). In mice fed a normal diet, most of the fluorescence signal from HABN−Cy5.5 was localized in the kidney, and minimal signal was observed in the normal liver (Figure 4b,c). In contrast, much higher fluorescence signals from HABN−Cy5.5 were found in the liver of mice kept on a CD-HFD than in their other organs (Figure 4b,c). These results show that HABNs administered intravenously accumulated in the fibrotic liver with minimal accumulation in the normal liver or other major organs (heart, lung, kidney, and spleen). Additionally, the fluorescence signals from HABN−Cy5.5 observed in the livers of mice kept on a CD-HFD were higher than the signals from PEG-BN−Cy5.5 in the livers of mice kept on a CD-HFD. This result indicates the critical role of the HA-shell in targeting the nanoparticles to the fibrotic liver.

Desmin is upregulated in activated HSCs and is widely used as a specific marker of activated HSCs.[47−51] To examine whether HABNs accumulated in desmin$^+$ activated HSCs *in vivo*, we intravenously administered HABN−Cy5.5 to mice fed a CD-HFD or a normal diet. Similar to previous reports,[48]

https://doi.org/10.1021/acsnano.3c06107
ACS Nano 2024, 18, 4704−4716

desmin expression was upregulated in the livers of mice kept on a CD-HFD, compared to the livers of normal mice (Figure 4d). Notably, no fluorescence signal from HABN−Cy5.5 was detectable in the livers of mice kept on a normal diet, and a strong fluorescence signal from HABN−Cy5.5 overlapping with desmin expression was found in the livers of mice kept on a CD-HFD (Figure 4d). In contrast, the fluorescence signal of PEG-BN−Cy5.5 was scarcely detected within the desmin-expressing regions of the livers of mice fed a CD-HFD (Figure 4e). Taken together, these results suggest that HABNs administered intravenously colocalize with desmin-expressing activated HSCs in fibrotic regions of the liver, probably due to the activated HSC-targeting ability of the HA shell.

HABNs Alleviate CD-HFD-Induced NASH Fibrosis. Based on the excellent HSC-specific antifibrotic activity of HABNs *in vitro* and their targeting of activated HSCs *in vivo*, we investigated the antifibrotic activity of HABNs *in vivo*. To investigate this, we fed mice a CD-HFD or a normal diet and then treated them with PBS, PEG-BNs, or HABNs. The treatment scheme is illustrated in Figure 5a. Western blotting assays and mRNA qRT PCR analyses of fibrotic liver tissue showed that the HABNs significantly decreased α-SMA, ACTA2, and PDGFB expression, indicating HSC inhibition consistent with the *in vitro* results (Figure 5b−e). In contrast, PEG-BNs did not significantly reduce the markers of activated HSCs. Furthermore, HABNs reduced the burden of deposited ECM, such as TIMP1 and collagens I and III, in the livers of mice kept on a CD-HFD, whereas the PEG-BNs showed minimal activity, suggesting that the HA shell rendered HABNs effective against liver fibrosis, presumably through the HA-mediated targeting of activated HSCs (Figure 5f−h).

Next, we examined whether HABNs could slow the progression of liver fibrosis in a murine CD-HFD-induced NASH fibrosis model. The treatment regimen is illustrated in Figure 6a. Mice fed a CD-HFD and treated with HABNs had significantly lower ALT and AST levels compared to mice fed a CD-HFD and treated with PBS, PEG-BNs, indicative of robust improvement in liver function (Figure 6b,c). To examine the extent of fibrosis *in vivo*, immunohistochemistry analyses were performed. The staining results indicate that the livers of mice fed a CD-HFD exhibited signs of NASH fibrosis, such as hepatocellular ballooning, extensive ECM formation, severe centrilobular necrosis, and immune cell infiltration (Figure 6d,f). Furthermore, compared with the control mice fed a CD-HFD, mice treated with PEG-BNs or HABNs had a reduced degree of liver fibrosis. Notably, the ballooning score (a key marker of NASH[52]) showed that the HABNs provided better efficacy than the PEG-BNs (Figure 6d,e). Also, NASH fibrotic mice treated with HABNs exhibited less collagen accumulation and thinner fibrotic septa than NASH fibrotic mice treated with PEG-BNs (Figure 6f,g). These results suggest that HABN-mediated, activated HSC-specific modulation is very effective in preventing the progression of NASH fibrosis. Lastly, repeated HABN treatments showed no evident indications of toxicity or pathology *in vivo* (Supplementary Figure 8).

Taken together, our results demonstrate that intravenously administered HABNs exert potent fibrotic modulation activity in a murine CD-HFD-induced NASH fibrosis model.

DISCUSSION

In this study, we present our discovery that the administration of antioxidant, CD44-targeting HABNs can specifically inhibit oxidative stress in activated HSCs, leading to the suppression of HSC activity and collagen deposition and consequently effectively preventing the progression of liver fibrosis (Figure 1). As activated HSCs are known to be a key contributor to liver fibrosis, various strategies targeting and modulating their activity have been investigated. Moreover, HSC activation, proliferation, and ECM production are closely linked to increased intracellular oxidative stress, making antioxidants a potential therapeutic option for liver fibrosis. Therefore, our objective was to target oxidative stress induced by activated HSCs with the aim of significantly reducing the progression of liver fibrosis.

Our results demonstrate that intravenously administered HABNs accumulated in activated HSCs in fibrotic liver areas *in vivo*, possibly due to an interaction between the HA shell of HABNs and CD44, which is overexpressed on activated HSCs (Figure 2, Figure 4, and Supplementary Figure 4). HSCs, a key player in the fibrosis process, exhibit high CD44 levels on their surfaces when activated.[11] HABNs exhibited significantly high internalization into activated HSCs with high CD44 expression both *in vitro* and *in vivo*, whereas PEG-BNs, which lack CD44 targeting capability, showed minimal localization in activated HSCs. Furthermore, pretreatment with free HA substantially reduced the rate of intracellular uptake of HABNs. These results emphasize the importance of the HA shell for targeting. Notably, HABNs did not accumulate among hepatocytes with low CD44 expression either *in vitro* or *in vivo*. These findings collectively support the effective targeting of intravenously administered HABNs to the liver, particularly to activated HSCs, in mice with CD-HFD-induced NASH fibrosis.

HABNs were taken up by activated HSCs, leading to inhibition of their activation and proliferation as well as collagen production, as evidenced by decreased expression of α-SMA, ACTA2, and PDGFB and reduced production of collagens I and III in LX-2 cells, HSC spheroids, and fibrotic murine livers (Figure 3c−f, Figure 5, and Supplementary Figure 5). This effect was likely due to the strong antioxidant activity of the BR core (Figure 3a,b). Oxidative stress plays a significant role in liver fibrogenesis. ROS are critical in promoting HSC activation, proliferation, migration, and collagen synthesis.[23−25] Because the BR core can scavenge ROS, HABNs significantly reduced the level of ROS production in activated HSCs. In contrast, HAoxBNs, which lack the ability to scavenge ROS, and PEG-BNs, which did not target activated HSCs, minimally affected the intracellular ROS levels in activated HSCs. Furthermore, the antioxidative CD44-targeting HABNs decreased the viability of activated LX-2 cells while inhibiting the activation of HSCs. Moreover, the HABNs significantly inhibited the production of collagens I and III in activated HSCs and murine fibrotic livers. In contrast, HAoxBNs and PEG-BNs minimally affected the activation and proliferation of HSCs and did not reduce the level of collagen expression in activated HSCs or murine fibrotic livers. The limited intracellular uptake, caused by a lack of the HA shell, is primarily responsible for the low activity of the non-CD44 targeting PEG-BNs, and the limited activity of the CD44-targeting HAoxBNs due to the oxidation of the BR core by ROS is strongly associated with their loss of antioxidant activity. Therefore, these results suggest that the intracellular uptake mediated by the HA shell and the subsequent antioxidant activity mediated by the BR core are both crucial to the antifibrotic activity of HABNs in activated HSCs.

https://doi.org/10.1021/acsnano.3c06107
ACS Nano 2024, 18, 4704−4716

The fibrosis process is largely driven by HSCs, which shift from a quiescent state to an activated state during persistent liver damage. Recent research has demonstrated that homeostatic ROS generation might protect the liver from the progression of liver fibrosis but amplified intracellular oxidative stress in activated HSCs significantly contributes to the fibrosis process. Those paradoxical roles of ROS in liver fibrosis[28,29] necessitate specific modulation of the activated HSCs that play the major role in liver fibrosis. Based on that information, we hypothesized that the antioxidant activated HSC-targeting HABNs would exhibit potent antifibrotic activity *in vivo*. In line with our hypothesis, intravenously administered HABNs demonstrated significantly better *in vivo* antifibrotic activity in a CD-HFD-induced murine NASH fibrosis model than PEG-BNs, which exhibited limited activity against activated HSCs *in vitro* and acted nonspecifically in fibrotic liver areas *in vivo* (Figure 6). Notably, the HABNs also modulated other NASH fibrosis-related symptoms, such as liver inflammation, ballooning of liver cells, and accumulation of fat in the liver.

In conclusion, this study presents targeted modulation of activated HSCs using an antioxidative activated HSC-targeting biocompatible nanomedicine that effectively prevented the progression of liver fibrosis. Oxidative stress within activated HSCs unquestionably plays a crucial role in liver fibrosis progression, although ROS have paradoxical roles in liver fibrosis and steatosis. Thus, specifically targeting and modulating activated HSCs using antioxidative approaches is imperative for treating liver fibrosis. Previous studies have used artificially synthesized materials with complex components and structures that require additional agents for HSC modulation. In contrast, our HABNs are composed of naturally occurring, biocompatible, and biodegradable materials: BR, an endogenous antioxidant and anti-inflammatory bile acid, and HA, an endogenous CD44-targeting glycosaminoglycan biopolymer. These features facilitate a straightforward, specific modulation of oxidative stress in activated HSCs, thereby preventing the progression of liver fibrosis. Importantly, these intriguing characteristics may enhance the clinical translational potential of our system. In summary, our findings strongly suggest that HABNs hold significant potential as an antioxidant, cytoprotective, targeted nanomedicine for various ROS-related diseases in which CD44-overexpressing cells play a pivotal role.

EXPERIMENTAL METHODS

Synthesis of the Hyaluronic Acid−Bilirubin (HA-BR) Conjugate. The HA-BR conjugate was synthesized from an acid form of HA and an amino-ethylene−bilirubin conjugate (AE-BR) using a slightly modified method based on the one previously described by Lee et al.[37,38] In brief, the acidic form of HA (80 μmol), prepared from the sodium salt form of HA (Lifecore Biomedical) using a dialysis method, and *N*-hydroxysuccinimide (NHS, 40 μmol) were mixed in DMSO (4.8 mL). After 1-ethyl-3-(3-dimethylaminopropyl)-carbodiimide (EDC, 140 μmol) was added, the solution was mixed for 10 min at RT. Then, AE-BR (20 μmol), prepared from BR and ethylenediamine using a simple EDC chemistry, was added. Subsequently, the mixture was stirred overnight at RT under nitrogen gas. Dialysis was carried out against 0.01 M NaOH 6 times for 20 h, water/acetonitrile (1:1) for 3 h, and then distilled water twice for 3 h. Finally, the native sodium salt form of HA-BR was obtained through lyophilization. ^{1}H NMR spectra were acquired on the ANANCE Neo 400 MHz system (Bruker). The BR portion of the HABNs was calculated by using UV/vis spectra from an ELISA reader (Multiskan GO with Cuvette function, Thermo Fisher Scientific).

Synthesis of PEGylated Bilirubin (PEG-BR). The PEG-BR conjugate was synthesized using a slightly modified method based on the one previously described by Lee et al.[37,38] For 10 min at RT, BR (75 μmol) and EDC (33.75 μmol) were mixed in DMSO (0.6 mL) containing triethylamine (225 μL) and NHS (52 μmol). Then, poly(ethylene glycol) 20K-amine (15 μmol, 20K-PEG-NH_2, Nanosoft Polymers) was added, and EDC/NHS chemistry was performed for 4 h under nitrogen gas. After addition of chloroform (50 mL), the organic solution was washed with 0.1 M HCl twice, 0.1 M $NaHCO_3$ twice, and distilled water twice (50 mL). After the resulting organic layer was evaporated, 50 mL of methanol was added. Unreacted remaining free BR was removed by centrifugation at 3000*g* for 10 min, and the supernatant was evaporated. Finally, PEG-BR was obtained through dialysis, following the procedure outlined in the HA-BR conjugate section and then lyophilization.

Synthesis of the HA-BR−Cy5.5 Conjugate. Cy5.5 conjugated HA-BR was synthesized using a slightly modified method based on the one previously described by Lee et al.[37,38] In brief, the acidic form of HA-BR (10.5 μmol), prepared from the native sodium salt form of HA-BR through dialysis against 0.01 M HCl and water, was dissolved in DMSO (0.8 mL) overnight. NHS (2 μmol) and EDC (2 μmol) were then added to the mixture and stirred for 10 min at RT. Cy5.5-NH_2 (0.1 μmol, AAT Bioquest) was then added and stirred overnight, followed by dialysis following the procedure outlined in the HA-BR conjugate section. The resulting solution underwent lyophilization, yielding the HA-BR−Cy5.5 conjugate.

Preparation of HABNs, PEG-BNs, and Cy5.5-tagged HABNs. HABNs, PEG-BNs, and Cy5.5-tagged HABNs were synthesized following a method previously described by Lee et al.[37,38] HA-BR, PEG-BR, or HA-BR−Cy5.5 were dissolved in water or PBS and then sonicated for 10 min at RT. Finally, HABNs, PEG-BNs, or Cy5.5-conjugated HABNs were obtained after filtration through a 0.45 μm filter membrane. The hydrodynamic size, zeta potential, and TEM morphology of HABNs, PEG-BNs, and Cy5.5-conjugated HABNs were examined using a Zetasizer Nano ZS90 (Malvern Instruments Ltd.) and a JEM-2100F (JEOL USA). Prepared HABNs, PEG-BNs, or Cy5.5-conjugated HABNs were diluted in PBS or a culture medium for further studies.

Cell Culture. The HepG2 human hepatocyte, AML12 murine hepatocyte, and LX-2 human hepatic stellate cell lines were obtained from ATCC. All cell lines tested negative for mycoplasma contamination. AML12 cells were cultured in DMEM/F12 (Welgene) containing 10% (v/v) fetal bovine serum (Corning), 5 mg/mL insulin, 5.5 μg/mL transferrin, 5 ng/mL selenium, and 40 ng/mL dexamethasone; HepG2 cells were cultured in RPMI medium (Welgene); and LX-2 cells were cultured in DMEM (Welgene) containing 10% (v/v) heat-inactivated fetal bovine serum (Gibco) and 100 IU/mL penicillin/streptomycin (Gibco) were cultured in a humidified 5% CO_2 atmosphere at 37 °C.

Preparation of the Native Polymer form of HAoxBR. To acquire HAoxBR, HABNs were oxidized with 2,2′-azobis(2-methylpropionamidine) dihydrochloride (AAPH, 100 mM) in water over 1 day at 37 °C. Then, dialysis was carried out against distilled water for 24 h to eliminate any remaining AAPH. Subsequently, the solution underwent lyophilization, yielding HAoxBR.

Preparation of NR@HABNs and NR@PEG-BNs. First, 0.5 mg of Nile red (NR, Tokyo Chemical Industry Co., Ltd.) was added to 1 mg of HABNs in 1 mL of chloroform, and then sonication was performed for 10 min at RT. After the organic solvent was evaporated, filtration was carried out through a filter membrane (0.45 μm) to eliminate any unloaded NR, resulting in the acquisition of evenly sized NR-loaded HABNs. The amount of NR loaded onto the nanoparticles was quantified using HPLC (Agilent 1260, Agilent Technologies).

Intracellular ROS. LX-2 cells were seeded in 96-well plates (4.0×10^4/well). After 1 day of incubation at 37 °C, the cells were treated with HABNs (0.5 mg/mL), HAoxBNs (0.5 mg/mL), PEG-BR (0.5 mg/mL), or fresh medium for 24 h. TGF-β1 (2 ng/mL) was added to the cells 9 h before the end of the nanoparticle treatments. The cells were then incubated for 1 h with diacetyldichlorofluorescein (DCFDA, 30 μM) in fresh medium. After washing the cells with PBS, we observed the fluorescence signals generated from DCFDA by

https://doi.org/10.1021/acsnano.3c06107
ACS Nano 2024, 18, 4704−4716

oxidation using a microplate reader (Twinfinite 200 PRO, Tecan) at 488 nm excitation and 525 nm emission.

***In Vitro* Confocal Microscopy.** For the CD44 expression and nanoparticle uptake assay, HepG2, AML12, and LX-2 cells were seeded on separate coverslips in 24 well plates (1.0×10^5/well). After a 2 day incubation at 37 °C, LX-2 cells were incubated with TGF-β1 (2 ng/mL, Bio-Techne) or control medium for 24 h. The cells were then treated with HABN−Cy5.5 (30 μg/mL), free NR (1 μg/mL), NR@HABNs (NR, 1 μg/mL; HABNs, 62.5 μg/mL), NR@PEG-BNs, and FITC-conjugated anti-CD44 antibody (1:100 dilution; Clone IM7, no. 103016, BioLegend), or control medium for 1 h. Subsequently, a fixation step with 4% paraformaldehyde was performed for 5 min. After being counterstained with Hoechst 33342 for 10 min and examined using a Nikon A1R confocal microscope. In the particle uptake competition assay, the cells were pretreated with 5 mg/mL free HA overnight before the nanoparticle treatment.

For the α-SMA and collagen-1 expression assay, LX-2 cells were treated with HABNs (0.2 mg/mL), HAoxBNs (0.2 mg/mL), PEG-BNs (0.2 mg/mL), or fresh medium for 24 h. TGF-β1 (2 ng/mL) was treated with the LX-2 cells 9 h before the end of the nanoparticle treatments. After the medium was replaced with fresh medium, LX-2 cells were further incubated overnight at 37 °C and then fixed with ice-cold 100% methanol for 5 min. After fixation, the cells were treated with PBS containing 0.25% Triton X-100 for 10 min and then treated with a blocking buffer [1% BSA and glycine (22.52 mg/mL) in PBST (PBS + 0.1% Tween 20)] for 0.5 h. The cells were then incubated with anti-α-SMA rabbit antibody (1:100 dilution; no. ab5694, Abcam) or anti-collagen-1 rabbit antibody (1:1000 dilution; no. ab34710, Abcam) in 1% BSA in PBST in a humidified chamber for 1 h at 37 °C. After washing with PBS, the cells were incubated in the dark with secondary anti-rabbit goat antibody (1:200 dilution; no. ab150077, Abcam) in 1% BSA in PBST in a humidified chamber for 1 h at 37 °C. The cells were then counterstained with Hoechst 33342 for 5 min. Finally, samples were examined by using a Nikon A1R confocal microscope.

***In Vitro* 3D Fibrosis Model Formation.** A 3D liver fibrosis spheroid model was prepared using a method described previously by Pingitore et al.[53] To form the 3D spheroids, AML12 and LX-2 cells (24:1 ratio) were seeded at 4.0×10^3 cells and cocultured in a 96-well round-bottom plate (no. 34896, SPL) with high-glucose DMEM (no. LM 001-05, Welgene) containing 10% (v/v) FBS (no. 35-015-CV, Corning). After spheroid formation was allowed for 8 days after seeding, the AML12/LX-2 spheroids were exposed to TGF-β (10 ng/mL) to mimic the pathophysiology of hepatic fibrosis.

***In Vitro* 3D Spheroid Intracellular ROS.** 3D spheroids that had been cultured for 8 days were treated with HABNs (10 μM), HAoxBNs (10 μM), or PEG-BNs (10 μM) for 48 h with or without TGF-β (10 ng/mL). On day 10, all spheroids were transferred into Nunc F96 MicroWell black polystyrene plates (no. 237105, Thermo Scientific) and incubated for 1 h with 20 μM dichlorodihydrofluorescein diacetate (DCFHDA) in fresh phenol-red-free medium. After we washed the spheroids with PBS, we measured the fluorescence signals generated from DCFHDA by oxidation using a microplate reader (Infinite 200 PRO, Tecan) with an excitation wavelength of 485 nm and an emission wavelength of 525 nm.

***In Vitro* 3D Spheroid Immunofluorescence Assay.** To form 3D spheroids, AML12 and LX-2 cells (in a 24:1 ratio) were seeded at 4.0×10^3 cells and cultured in a 96-well round-bottom plate for 8 days. On day 8, the 3D spheroids were treated with HABNs (10 μM), HAoxBNs (10 μM), or PEG-BNs (10 μM) for 48 h in the absence or presence of TGF-β (10 ng/mL). The 3D spheroids were fixed in a 4% paraformaldehyde solution for 1 h and subsequently incubated overnight in a 20% sucrose solution. Then, all spheroids were embedded in the OCT compound and prepared as frozen sections (8 μm thick). After being washed with 1× ice-cold PBS, the sections were blocked using a blocking solution (1% BSA, 300 mM glycine, PBST) and incubated with α-SMA antibody (1:1000 dilution; no. ab5694, Abcam) or collagen-1 antibody (1:1000 dilution; no. ab34710, Abcam) in PBST for 2 h. After being washed again with 1× PBS, the spheroids were treated with Alexa Fluor 488-conjugated secondary antibody (1:100, no. 4412, Cell Signaling Technology) for 1 h. After being washed with PBS, the spheroids were counterstained with DAPI (0.1 μg/mL in PBS) for 10 min. Finally, the samples were monitored by using a fluorescence microscope (Apotome, Carl Zeiss Co. Ltd.) and analyzed with Zen Pro software.

CCK-8 Assay. LX-2 or AML12 cells were seeded onto 96-well plates (1×10^4/well). After 1 day of incubation at 37 °C, the cells were treated with 100 μL of HABNs (50, 100, 200, 400 μg/mL) or fresh medium for 15 h. TGF-β1 (2 ng/mL) was treated with the LX-2 cells or AML12 cells 9 h before the end of the nanoparticle treatments. After the removal of the medium, the cells were treated with fresh culture medium supplemented with CCK-8 (10:1 ratio, Abbkine) for 1−2 h at 37 °C. Finally, an ELISA reader (Multiskan GO with Cuvette function, Thermo Fisher Scientific) was used to measure the absorbance at 450 nm.

Animals. All work performed on animals was in accordance with and approved by the Institutional Animal Care & Use Committee (IACUC) at Ewha Womans University (IACUC No. 19-041). All animals were obtained from Raon-bio (Korea) as mixed littermates and housed under pathogen-free conditions in the animal facility at the College of Pharmacy, Ewha Womans University.

Preparation of Cy5.5-Loaded PEGylated Bilirubin Nanoparticles (Cy5.5@PEG-BN). First, Cy5.5-COOH (0.5 mg, HY-D1040, MedChemExpress) was added to PEG-BNs (1 mg/mL) in chloroform, and then sonication was performed for 10 min at RT. After evaporation of the organic solvent, we performed dialysis overnight against distilled water to remove the remaining unloaded Cy5.5. The amount of Cy5.5 loaded onto the nanoparticles was measured using UV/vis spectra from an ELISA reader (Multiskan GO with a Cuvette function, Thermo Fisher Scientific).

***In Vivo* Imaging System (IVIS) Imaging.** To investigate the distribution of the HABNs and PEG-BNs in the liver, C57BL/6J mice (male, 6-week-old) kept on a normal diet (standard mouse pellet) or CD-HFD (L-amino acid diet containing 60% of calories from fat, with 0.1% methionine and devoid of additional choline, no. A06071302, Research Diet) for 6 weeks were iv-injected with 3.5 mg/kg of HABN−Cy5.5 (with corresponding amount of 4.3 μg of free Cy5.5 in 1 mg of HABN−Cy5.5) or 3 mg/kg of Cy5.5-loaded PEG-BN (with a mass of free Cy5.5 equiv to that in the HABN−Cy5.5) on day 42. Six hours after treatment, all mice were sacrificed, and major organs were excised immediately. The fluorescence intensities of the major organs were monitored using an *in vivo* imaging system (IVIS, PerkinElmer) under a Cy5.5 filter channel.

***In Vivo* Immunofluorescence Assay.** Liver tissues were freshly excised from the mice, fixed in 4% paraformaldehyde, and then prepared as frozen tissue sections. The sections were incubated with PBS containing 0.1−0.25% Triton X-100 (Sigma-Aldrich) for 10 min. The sections were then blocked with blocking solution (1% BSA, 300 mM glycine, PBST) and incubated with antibody (desmin−FITC, no. NBP2-54503F, Novus Biologicals) in PBST containing 1% BSA overnight at 4 °C. Following another wash with 1× PBS, DAPI solution (0.1 μg/mL) was added for 10 min. The samples were monitored using a fluorescence microscope (Apotome, Carl Zeiss Co., Ltd.) and analyzed with Zen pro software.

***In Vivo* Hepatic Fibrosis Model Study.** C57BL/6J (male, 6-week-old) mice kept on a normal diet or a CD-HFD for 6 weeks were administered 12 mg/kg (iv) HABNs, PEG-BNs, or PBS every 3 days for a total of 7 times. On day 42, blood was collected for the blood parameter analysis, and the murine livers were excised. Liver weight and size were assessed, and the liver tissues were used for further *in vivo* tissue analyses.

***In Vivo* Western Blot Analyses.** Liver tissues were lysed in lysis buffer (20 mM HEPES at pH 7.0, 0.15 M NaCl, 10% glycerol, 0.5% NP40, 1% phenylmethylsulfonyl fluoride (PMSF), 1% cocktail inhibitor (GenDEPOT), 1% TritonX-100, 1 mM EDTA, 1 mM EGTA, 1 mM sodium orthovanadate, and 5 mM sodium fluoride). The Western blot analysis procedures followed the general protocols described elsewhere. Protein bands were visualized using a LAS-3000 instrument (FUJIFILM Corporation) with ECL solution reagent (GE

https://doi.org/10.1021/acsnano.3c06107
ACS Nano 2024, 18, 4704−4716

Healthcare). Images were captured and analyzed with Multi-Gauge V3.0 software. Anti-α-SMA antibody (no. 19245) and anti-vinculin antibody (no. PM088) were from Cell Signaling Technology and MBL, respectively.

***In Vivo* Immunohistochemistry Assay.** Liver tissues freshly excised from mice were immediately fixed in 4% paraformaldehyde and used to make paraffin-embedded block sections for immunohistochemistry (IHC). IHC procedures followed the general protocols described elsewhere. Sections were stained with hematoxylin (no. HMM999, Scy Tek, Inc.) and eosin (no. 318906, Sigma-Aldrich) or Sirius red (Picro Sirius red stain kit, no. ab150681, Abcam) according to the manufacturers' instructions. All images were captured using a microscope (Carl Zeiss Co. Ltd., Jena, Germany) at 200× magnification at the Ewha Drug Development Research Core Center and analyzed with ImageJ software. IHC staining was evaluated quantitatively using the IHC score. For this staining, α-SMA antibody (no. 19245, Cell Signaling Technology) was diluted according to the manufacturer's recommendations.

Quantitative Real-Time PCR (qRT PCR) Assay. Total RNA was extracted from liver tissues using Tri-RNA reagent (FAVORGEN Biotech Corp.), and complementary DNA was prepared using a PrimeScript RT reagent kit (no. RR037A, Takara Bio Inc.) following the manufacturers' instructions. Quantitative analyses of the specified genes were performed using a TB Green Premix Ex *Taq*II (no. RR820A, Takara Bio Inc.). PCR amplification was carried out using a CFX96 real-time PCR detection system (Bio-Rad). The relative quantity of mRNA was normalized to that of GAPDH. All qRT PCR primer sequences are listed here: GAPDH-forward: AATGGTGAAGGTCGGTGTG, GAPDH-reverse: GTGGAGTCATACTGGAACATGTAG; TIMP1-forward: GCAACTCGGACCTGGTCATAA, TIMP1-reverse: CGGCCCGTGATGAGAAACT; PDGFB-forward: CATCCGCTCCTTTGATGATCTT, PDGFB-reverse: GTGCTCGGGTCATGTTCAAGT; COL1A1-forward: ATGGATCGTTCGAGTACG, COL1A1-reverse: TCAGCTGGATAGCGACATCG; COL3A1-forward: CTGTAACATGGAAACTGGGGAAA, COL3A1-reverse: CCATAGCTGAACTGAAAACCAC; ACTA2-forward: GTCCCAGACATCAGGGAGTAA, ACTA2-reverse: TCGGATACTTCAGCGTCAGGA.

***In Vivo* Blood Parameter Analysis.** Collected blood was added to EDTA-coated microcentrifuge tubes (Zhejiang), followed by centrifugation at 10,000 rpm for 10 min. Plasma levels of aspartate transaminase (AST) and alanine transaminase (ALT) were quantified using a FUJI-DRI-CHEM NX500i (FUJIFILM Corporation) according to the manufacturer's instructions.

***In Vivo* Toxicity Test.** Six-week-old male C57BL/6 mice were iv-injected with HABNs (50 mg/kg) or PBS a total of 5 times ever other day. The behavior and weight of mice were monitored for 1 week. After the mice were euthanized, major organs were excised. After fixation with 4% (v/v) buffered formalin and 70% (v/v) alcohol and embedding in paraffin, the tissue underwent sectioning and H&E staining processes. Finally, the samples were microscopically analyzed.

Statistical Analysis. All experiments were conducted at least twice with duplicate repeated measures. The results are presented as mean ± SEM. A one-way ANOVA followed by Tukey's HSD multiple comparison post hoc test was used to assess differences among groups. Statistical significance is indicated as $*p < 0.05$, $**p < 0.01$, $***p < 0.001$, and $****p < 0.0001$. GraphPad Prism 8.0 (GraphPad Software, La Jolla, CA) was used for the statistical analyses. Experiments were independently replicated several times, as specified in each figure legend.

ASSOCIATED CONTENT

Supporting Information

The Supporting Information is available free of charge at https://pubs.acs.org/doi/10.1021/acsnano.3c06107.

Synthesis of hyaluronic acid-bilirubin conjugate (HA-BR); characterization of HA-BR; preparation and characterization of hyaluronic acid−bilirubin nanoparticles (HABNs); HABN targeting of TGF-β-activated LX-2 cells; HABN antifibrotic activity in the *in vitro* 3D fibrosis model consisting of hepatocytes and HSCs; HABN lack of toxicity in quiescent LX-2 and AML12 cells; schematic illustration of the synthesis of HABN−Cy5.5; safety profile of HABN therapy (PDF)

AUTHOR INFORMATION

Corresponding Authors

Youngjoo Kwon − *Department of Pharmacy, College of Pharmacy, Ewha Womans University, Seoul 03760, South Korea;* orcid.org/0000-0001-6256-3042; Email: ykwon@ewha.ac.kr

Yonghyun Lee − *Department of Pharmacy, College of Pharmacy, Ewha Womans University, Seoul 03760, South Korea;* orcid.org/0000-0002-2728-9698; Email: y.lee@ewha.ac.kr

Authors

Jongyoon Shinn − *Department of Pharmacy, College of Pharmacy, Ewha Womans University, Seoul 03760, South Korea*

Seojeong Park − *Department of Pharmacy, College of Pharmacy, Ewha Womans University, Seoul 03760, South Korea*

Seonju Lee − *Department of Pharmacy, College of Pharmacy, Ewha Womans University, Seoul 03760, South Korea*

Nayoon Park − *Department of Pharmacy, College of Pharmacy, Ewha Womans University, Seoul 03760, South Korea*

Seojeong Kim − *Department of Pharmacy, College of Pharmacy, Ewha Womans University, Seoul 03760, South Korea*

Seohui Hwang − *Department of Pharmacy, College of Pharmacy, Ewha Womans University, Seoul 03760, South Korea*

James J. Moon − *Department of Pharmaceutical Sciences, Biointerfaces Institute, Department of Biomedical Engineering, and Department of Chemical Engineering, University of Michigan, Ann Arbor, Michigan 48109, United States*

Complete contact information is available at: https://pubs.acs.org/10.1021/acsnano.3c06107

Author Contributions

[▽]J.S. and S.P. contributed equally to this work. J.S., S.P., Y.K., and Y.L. designed the experiments. J.S. and S.P. performed most experiments. S.L., N.P., S.K., and S.H. aided with some experiments. J.S., S.P., Y.K., and J.M. analyzed the data. J.M. aided with editing the manuscript. Y.L. supervised the project and wrote the manuscript.

Notes

The authors declare no competing financial interest.

ACKNOWLEDGMENTS

The Basic Science Research Program through the National Research Foundation of Korea (NRF) funded by the Ministry of Education supported this research (2022R1C1C1003141, 2022M3H4A1A03067401). This research was also supported by a grant of the Korea Health Technology R&D Project through the Korea Health Industry Development Institute (KHIDI), funded by the Ministry of Health & Welfare,

Republic of Korea (RS-2023-00265981). This work was supported by grants from National Research Foundation of Korea (NRF) funded by the Korean government (MSIT) (2018R1A5A2025286). A Korea Basic Science Institute (National Research Facilities and Equipment Center) grant funded by the Ministry of Education supported this research (2023R1A6C103A026, 2021R1A6C101A442). The authors thank the Ewha Drug Development Research Core Center and Ewha Fluorescence Core Imaging Center for their help with the NMR, UV/vis spectrophotometry, HPLC, ivIS, and confocal analyses. The authors thank Seon Ah Lee for her technical help with the confocal microscopy analyses.

REFERENCES

(1) Henderson, N. C.; Rieder, F.; Wynn, T. A. Fibrosis: from mechanisms to medicines. *Nature* **2020**, *587* (7835), 555−566.
(2) Tsuchida, T.; Friedman, S. L. Mechanisms of hepatic stellate cell activation. *Nat. Rev. Gastroenterol Hepatol* **2017**, *14* (7), 397−411.
(3) Bottcher, K.; Pinzani, M. Pathophysiology of liver fibrosis and the methodological barriers to the development of anti-fibrogenic agents. *Adv. Drug Deliv Rev.* **2017**, *121*, 3−8.
(4) Ribera, J.; Vilches, C.; Sanz, V.; de Miguel, I.; Portoles, I.; Cordoba-Jover, B.; Prat, E.; Nunes, V.; Jimenez, W.; Quidant, R.; et al. Treatment of Hepatic Fibrosis in Mice Based on Targeted Plasmonic Hyperthermia. *ACS Nano* **2021**, *15* (4), 7547−7562.
(5) Qiao, J. B.; Fan, Q. Q.; Zhang, C. L.; Lee, J.; Byun, J.; Xing, L.; Gao, X. D.; Oh, Y. K.; Jiang, H. L. Hyperbranched lipoid-based lipid nanoparticles for bidirectional regulation of collagen accumulation in liver fibrosis. *J. Controlled Release* **2020**, *321*, 629−640.
(6) Libbrecht, L.; Desmet, V.; Roskams, T. Preneoplastic lesions in human hepatocarcinogenesis. *Liver Int.* **2005**, *25* (1), 16−27.
(7) Fabregat, I.; Roncero, C.; Fernandez, M. Survival and apoptosis: a dysregulated balance in liver cancer. *Liver Int.* **2007**, *27* (2), 155−162.
(8) Flamm, S. L.; Yang, Y. X.; Singh, S.; Falck-Ytter, Y. T.; The AGA Institute Clinical Guidelines Committee. American Gastroenterological Association Institute Guidelines for the Diagnosis and Management of Acute Liver Failure. *Gastroenterology* **2017**, *152* (3), 644−647.
(9) Cheng, Q.; Li, C.; Yang, C. F.; Zhong, Y. J.; Wu, D.; Shi, L.; Chen, L.; Li, Y. W.; Li, L. Methyl ferulic acid attenuates liver fibrosis and hepatic stellate cell activation through the TGF-beta1/Smad and NOX4/ROS pathways. *Chem. Biol. Interact* **2019**, *299*, 131−139.
(10) Beljaars, L.; Molema, G.; Schuppan, D.; Geerts, A.; De Bleser, P. J.; Weert, B.; Meijer, D. K.; Poelstra, K. Successful targeting to rat hepatic stellate cells using albumin modified with cyclic peptides that recognize the collagen type VI receptor. *J. Biol. Chem.* **2000**, *275* (17), 12743−12751.
(11) Hochst, B.; Schildberg, F. A.; Sauerborn, P.; Gabel, Y. A.; Gevensleben, H.; Goltz, D.; Heukamp, L. C.; Turler, A.; Ballmaier, M.; Gieseke, F.; et al. Activated human hepatic stellate cells induce myeloid derived suppressor cells from peripheral blood monocytes in a CD44-dependent fashion. *J. Hepatol* **2013**, *59* (3), 528−535.
(12) Li, W.; Zhou, C.; Fu, Y.; Chen, T.; Liu, X.; Zhang, Z.; Gong, T. Targeted delivery of hyaluronic acid nanomicelles to hepatic stellate cells in hepatic fibrosis rats. *Acta Pharm. Sin B* **2020**, *10* (4), 693−710.
(13) Li, F.; Sun, J. Y.; Wang, J. Y.; Du, S. L.; Lu, W. Y.; Liu, M.; Xie, C.; Shi, J. Y. Effect of hepatocyte growth factor encapsulated in targeted liposomes on liver cirrhosis. *J. Controlled Release* **2008**, *131* (1), 77−82.
(14) Hao, Y.; Song, K.; Tan, X.; Ren, L.; Guo, X.; Zhou, C.; Li, H.; Wen, J.; Meng, Y.; Lin, M.; et al. Reactive Oxygen Species-Responsive Polypeptide Drug Delivery System Targeted Activated Hepatic Stellate Cells to Ameliorate Liver Fibrosis. *ACS Nano* **2022**, *16* (12), 20739−20757.
(15) Liang, S.; Ma, H. Y.; Zhong, Z.; Dhar, D.; Liu, X.; Xu, J.; Koyama, Y.; Nishio, T.; Karin, D.; Karin, G.; et al. NADPH Oxidase 1 in Liver Macrophages Promotes Inflammation and Tumor Development in Mice. *Gastroenterology* **2019**, *156* (4), 1156−1172.
(16) Chen, Y. N.; Hsu, S. L.; Liao, M. Y.; Liu, Y. T.; Lai, C. H.; Chen, J. F.; Nguyen, M. T.; Su, Y. H.; Chen, S. T.; Wu, L. C. Ameliorative Effect of Curcumin-Encapsulated Hyaluronic Acid-PLA Nanoparticles on Thioacetamide-Induced Murine Hepatic Fibrosis. *Int. J. Environ. Res. Public Health* **2017**, *14* (1), 11.
(17) Sanyal, A. J.; Chalasani, N.; Kowdley, K. V.; McCullough, A.; Diehl, A. M.; Bass, N. M.; Neuschwander-Tetri, B. A.; Lavine, J. E.; Tonascia, J.; Unalp, A.; et al. Pioglitazone, Vitamin E, or Placebo for Nonalcoholic Steatohepatitis. *New Engl J. Med.* **2010**, *362* (18), 1675−1685.
(18) Nguyen-Khac, E.; Thevenot, T.; Piquet, M. A.; Benferhat, S.; Goria, O.; Chatelain, D.; Tramier, B.; Dewaele, F.; Ghrib, S.; Rudler, M.; et al. Glucocorticoids plus N-Acetylcysteine in Severe Alcoholic Hepatitis. *New Engl J. Med.* **2011**, *365* (19), 1781−1789.
(19) Chen, Z.; Tian, R. F.; She, Z. G.; Cai, J. J.; Li, H. L. Role of oxidative stress in the pathogenesis of nonalcoholic fatty liver disease. *Free Radical Bio Med.* **2020**, *152*, 116−141.
(20) Richter, K.; Kietzmann, T. Reactive oxygen species and fibrosis: further evidence of a significant liaison. *Cell Tissue Res.* **2016**, *365* (3), 591−605.
(21) Sanchez-Valle, V.; Chavez-Tapia, N. C.; Uribe, M.; Mendez-Sanchez, N. Role of oxidative stress and molecular changes in liver fibrosis: a review. *Curr. Med. Chem.* **2012**, *19* (28), 4850−4860.
(22) Mohamed, S. H.; Shahat, A. A.; Mohamed, M. R.; Khalil, W. K. B.; Salem, A. M.; Farrag, A. R. H.; Ahmed, H. H. leaves extract ameliorates high fat diet-induced nonalcoholic steatohepatitis in rats: analysis of potential mechanisms. *J. Pharm. Invest* **2021**, *51* (2), 183−197.
(23) Kong, M.; Chen, X.; Lv, F.; Ren, H.; Fan, Z.; Qin, H.; Yu, L.; Shi, X.; Xu, Y. Serum response factor (SRF) promotes ROS generation and hepatic stellate cell activation by epigenetically stimulating NCF1/2 transcription. *Redox Biol.* **2019**, *26*, 101302.
(24) Weiskirchen, R.; Tacke, F. Cellular and molecular functions of hepatic stellate cells in inflammatory responses and liver immunology. *Hepatobiliary Surg Nutr* **2014**, *3* (6), 344−363.
(25) Nieto, N.; Friedman, S. L.; Cederbaum, A. I. Stimulation and proliferation of primary rat hepatic stellate cells by cytochrome P450 2E1-derived reactive oxygen species. *Hepatology* **2002**, *35* (1), 62−73.
(26) Luangmonkong, T.; Suriguga, S.; Mutsaers, H. A. M.; Groothuis, G. M. M.; Olinga, P.; Boersema, M. Targeting Oxidative Stress for the Treatment of Liver Fibrosis. *Rev. Physiol Biochem Pharmacol* **2018**, *175*, 71−102.
(27) Gandhi, C. R. Oxidative Stress and Hepatic Stellate Cells: A PARADOXICAL RELATIONSHIP. *Trends Cell Mol. Biol.* **2012**, *7*, 1−10.
(28) Tsedensodnom, O.; Sadler, K. C. ROS: Redux and Paradox in Fatty Liver Disease. *Hepatology* **2013**, *58* (4), 1210−1212.
(29) Sakaguchi, T. F. Homeostatic Generation of Reactive Oxygen Species Protects Liver from Hepatic Steatosis in Zebrafish. *Free Radical Bio Med.* **2012**, *53*, S36−S36.
(30) Surendran, S. P.; Thomas, R. G.; Moon, M. J.; Park, R.; Lee, J. H.; Jeong, Y. Y. A bilirubin-conjugated chitosan nanotheranostics system as a platform for reactive oxygen species stimuli-responsive hepatic fibrosis therapy. *Acta Biomater* **2020**, *116*, 356−367.
(31) Kurniawan, D. W.; Booijink, R.; Pater, L.; Wols, I.; Vrynas, A.; Storm, G.; Prakash, J.; Bansal, R. Fibroblast growth factor 2 conjugated superparamagnetic iron oxide nanoparticles (FGF2-SPIONs) ameliorate hepatic stellate cells activation in vitro and acute liver injury in vivo. *J. Controlled Release* **2020**, *328*, 640−652.
(32) He, Q.; Zhang, J.; Chen, F.; Guo, L.; Zhu, Z.; Shi, J. An anti-ROS/hepatic fibrosis drug delivery system based on salvianolic acid B loaded mesoporous silica nanoparticles. *Biomaterials* **2010**, *31* (30), 7785−7796.
(33) Salomone, F.; Li Volti, G.; Rosso, C.; Grosso, G.; Bugianesi, E. Unconjugated bilirubin, a potent endogenous antioxidant, is decreased in patients with non-alcoholic steatohepatitis and advanced fibrosis. *J. Gastroenterol. Hepatol.* **2013**, *28* (7), 1202−1208.

https://doi.org/10.1021/acsnano.3c06107
ACS Nano 2024, 18, 4704−4716

(34) Tang, Y.; Zhang, Q.; Zhu, Y.; Chen, G.; Yu, F. Low concentrations of bilirubin inhibit activation of hepatic stellate cells in vitro. *Mol. Med. Rep* **2017**, *15* (4), 1647−1653.
(35) Weaver, L.; Hamoud, A. R.; Stec, D. E.; Hinds, T. D., Jr. Biliverdin reductase and bilirubin in hepatic disease. *Am. J. Physiol Gastrointest Liver Physiol* **2018**, *314* (6), G668−G676.
(36) Sedlak, T. W.; Saleh, M.; Higginson, D. S.; Paul, B. D.; Juluri, K. R.; Snyder, S. H. Bilirubin and glutathione have complementary antioxidant and cytoprotective roles. *Proc. Natl. Acad. Sci. U. S. A.* **2009**, *106* (13), 5171−5176.
(37) Lee, Y.; Shinn, J.; Xu, C.; Dobson, H. E.; Neamati, N.; Moon, J. J. Hyaluronic acid-bilirubin nanomedicine-based combination chemo-immunotherapy. *Nat. Commun.* **2023**, *14* (1), 4771.
(38) Lee, Y.; Sugihara, K.; Gillilland, M. G., 3rd; Jon, S.; Kamada, N.; Moon, J. J. Hyaluronic acid-bilirubin nanomedicine for targeted modulation of dysregulated intestinal barrier, microbiome and immune responses in colitis. *Nat. Mater.* **2020**, *19* (1), 118−126.
(39) Cho Lee, A.-R. Size matters: differential property of hyaluronan and its fragments in the skin- relation to pharmacokinetics, immune activity and wound healing. *J. Pharm. Invest* **2023**, *53* (3), 357−376.
(40) Stocker, R.; Yamamoto, Y.; McDonagh, A. F.; Glazer, A. N.; Ames, B. N. Bilirubin is an antioxidant of possible physiological importance. *Science* **1987**, *235* (4792), 1043−1046.
(41) Lee, Y. S.; Seki, E. In Vivo and In Vitro Models to Study Liver Fibrosis: Mechanisms and Limitations. *Cell Mol. Gastroenterol Hepatol* **2023**, *16* (3), 355−367.
(42) Barbero-Becerra, V. J.; Giraudi, P. J.; Chávez-Tapia, N. C.; Uribe, M.; Tiribelli, C.; Rosso, N. The interplay between hepatic stellate cells and hepatocytes in an model of NASH. *Toxicol in Vitro* **2015**, *29* (7), 1753−1758.
(43) Xu, L.; Hui, A. Y.; Albanis, E.; Arthur, M. J.; O'Byrne, S. M.; Blaner, W. S.; Mukherjee, P.; Friedman, S. L.; Eng, F. J. Human hepatic stellate cell lines, LX-1 and LX-2: new tools for analysis of hepatic fibrosis. *Gut* **2005**, *54* (1), 142−151.
(44) Carpino, G.; Morini, S.; Ginanni Corradini, S.; Franchitto, A.; Merli, M.; Siciliano, M.; Gentili, F.; Onetti Muda, A.; Berloco, P.; Rossi, M.; et al. Alpha-SMA expression in hepatic stellate cells and quantitative analysis of hepatic fibrosis in cirrhosis and in recurrent chronic hepatitis after liver transplantation. *Dig Liver Dis* **2005**, *37* (5), 349−356.
(45) Smith-Cortinez, N.; Fagundes, R. R.; Gomez, V.; Kong, D.; de Waart, D. R.; Heegsma, J.; Sydor, S.; Olinga, P.; de Meijer, V. E.; Taylor, C. T.; et al. Collagen release by human hepatic stellate cells requires vitamin C and is efficiently blocked by hydroxylase inhibition. *FASEB J.* **2021**, *35* (2), e21219.
(46) Matsumoto, M.; Hada, N.; Sakamaki, Y.; Uno, A.; Shiga, T.; Tanaka, C.; Ito, T.; Katsume, A.; Sudoh, M. An improved mouse model that rapidly develops fibrosis in non-alcoholic steatohepatitis. *Int. J. Exp Pathol* **2013**, *94* (2), 93−103.
(47) Yang, W.; He, H.; Wang, T.; Su, N.; Zhang, F.; Jiang, K.; Zhu, J.; Zhang, C.; Niu, K.; Wang, L.; et al. Single-Cell Transcriptomic Analysis Reveals a Hepatic Stellate Cell-Activation Roadmap and Myofibroblast Origin During Liver Fibrosis in Mice. *Hepatology* **2021**, *74* (5), 2774−2790.
(48) Hoffmann, C.; Djerir, N. E.; Danckaert, A.; Fernandes, J.; Roux, P.; Charrueau, C.; Lachages, A. M.; Charlotte, F.; Brocheriou, I.; Clement, K.; et al. Hepatic stellate cell hypertrophy is associated with metabolic liver fibrosis. *Sci. Rep-Uk* **2020**, *10* (1), 3850.
(49) Zhang, D.; Zhuang, R.; Guo, Z.; Gao, M.; Huang, L.; You, L.; Zhang, P.; Li, J.; Su, X.; Wu, H.; et al. Desmin- and vimentin-mediated hepatic stellate cell-targeting radiotracer (99m)Tc-GlcNAc-PEI for liver fibrosis imaging with SPECT. *Theranostics* **2018**, *8* (5), 1340−1349.
(50) Kim, S. J.; Ise, H.; Goto, M.; Akaike, T. Interactions of vimentin- or desmin-expressing liver cells with N-acetylglucosamine-bearing polymers. *Biomaterials* **2012**, *33* (7), 2154−2164.
(51) Niki, T.; Pekny, M.; Hellemans, K.; De Bleser, P.; Van den Berg, K.; Vaeyens, F.; Quartier, E.; Schuit, F.; Geerts, A. Class VI intermediate filament protein nestin is induced during activation of rat hepatic stellate cells. *Hepatology* **1999**, *29* (2), 520−527.
(52) Caldwell, S.; Ikura, Y.; Dias, D.; Isomoto, K.; Yabu, A.; Moskaluk, C.; Pramoonjago, P.; Simmons, W.; Scruggs, H.; Rosenbaum, N.; et al. Hepatocellular ballooning in NASH. *J. Hepatol* **2010**, *53* (4), 719−723.
(53) Pingitore, P.; Sasidharan, K.; Ekstrand, M.; Prill, S.; Linden, D.; Romeo, S. Human Multilineage 3D Spheroids as a Model of Liver Steatosis and Fibrosis. *Int. J. Mol. Sci.* **2019**, *20* (7), 1629.

https://doi.org/10.1021/acsnano.3c06107
ACS Nano 2024, 18, 4704−4716